



# **JGR** Solid Earth

## RESEARCH ARTICLE

10.1029/2021JB022646

#### **Key Points:**

- Magnetomineralogy and magnetic property of MORB vary with progressive high-temperature hydrothermal alteration
- Exsolution superimposed on titanomagnetite dissolution, producing a dual Verwey transition feature in partially chloritized basalts
- Hydrothermal alteration may have contributed to the long-term magnetization variations of oceanic basalts

#### **Supporting Information:**

Supporting Information may be found in the online version of this article.

#### Correspondence to:

L. Chang and C. Tao, liao.chang@pku.edu.cn; taochunhuimail@163.com

#### Citation:

Wang, S., Chang, L., Tao, C., Bilardello, D., Liu, L., & Wu, T. (2021). Seafloor magnetism under hydrothermal alteration: Insights from magnetomineralogy and magnetic properties of the Southwest Indian Ridge basalts. *Journal of Geophysical Research: Solid Earth*, 126, e2021JB022646. https://doi.org/10.1029/2021JB022646

Received 21 JUN 2021 Accepted 12 DEC 2021

#### **Author Contributions:**

**Conceptualization:** Shishun Wang, Liao Chang

Formal analysis: Shishun Wang Funding acquisition: Liao Chang, Chunhui Tao

**Investigation:** Shishun Wang, Liao Chang, Dario Bilardello

**Methodology:** Shishun Wang, Liao Chang

**Project Administration:** Liao Chang, Chunhui Tao

Resources: Liao Chang
Supervision: Liao Chang
Validation: Shishun Wang
Visualization: Shishun Wang Lou

Visualization: Shishun Wang, Long Liu, Tao Wu

© 2021. American Geophysical Union. All Rights Reserved.

# Seafloor Magnetism Under Hydrothermal Alteration: Insights From Magnetomineralogy and Magnetic Properties of the Southwest Indian Ridge Basalts

Shishun Wang<sup>1</sup>, Liao Chang<sup>1,2</sup>, Chunhui Tao<sup>3,4</sup>, Dario Bilardello<sup>5</sup>, Long Liu<sup>3</sup>, and Tao Wu<sup>3</sup>

<sup>1</sup>Laboratory of Orogenic Belts and Crustal Evolution, School of Earth and Space Sciences, Peking University, Beijing, China, <sup>2</sup>Laboratory for Marine Geology, Qingdao National Laboratory for Marine Science and Technology, Qingdao, China, <sup>3</sup>Key Laboratory of Submarine Geosciences, Second Institute of Oceanography, Ministry of Natural Resources, Hangzhou, China, <sup>4</sup>School of Oceanography, Shanghai Jiao Tong University, Shanghai, China, <sup>5</sup>Institute for Rock Magnetism, Department of Earth and Environmental Sciences, University of Minnesota, Minneapolis, MN, USA

Abstract Titanomagnetites in mid-ocean ridge basalt (MORB) experience variable post crystallization alterations associated with seafloor tectonic and environmental processes. Compared to low-temperature oxidation, seafloor hydrothermal alteration is thought to be more destructive but its magnetic aftermaths are insufficiently documented. Here we present comprehensive rock magnetic and electron microscopic analyses of fresh and hydrothermally-altered MORBs dredged from the Longqi and Yuhuang hydrothermal fields, Southwest Indian Ridge. We observe large variations in magnetic properties of fresh MORBs, originated from relative proportions of nano-scale single-domain to vortex state and micron-scale vortex to multi-domain state dendritic titanomagnetites. Progressive hydrothermal alteration produces secondary magnetite through recrystallization of exsolved and dissolved Fe from primary titanomagnetite. Exsolution is evident by a dual Verwey transition signature and coexisting Ti-poor titanomagnetites and sphenes in partially chloritized basalts. A schematic model is proposed to explain the variations in magnetomineralogy and magnetic properties with progressive hydrothermal alteration. Intermediate hydrothermal alteration products retain a secondary chemical remanent magnetization (CRM) which is related to the long-term magnetization variations in oceanic basalts. The established framework allows characterizing MORB hydrothermal alteration and ultimately contributes to resolving the complexity of seafloor magnetism.

**Plain Language Summary** Seafloor magnetism is essential for understanding geodynamics and resource prospecting. Near the seafloor high-temperature hydrothermal fields that host "black smokers", the primary titanomagnetites in oceanic basalts experience complicated alterations that profoundly change seafloor magnetic anomalies. This study investigates the alteration of titanomagnetite through fluid-rock interactions in such seafloor settings. We find titanomagnetite is disassembled into Fe-rich and Ti-rich phases when interacting with fluids, causing a series of magnetic property variations. A schematic model is proposed to explain how high-temperature fluid-rock interactions gradually destroy seafloor magnetism. This model improves our understanding of seafloor magnetism from the perspective of hydrothermal alterations, which is important for applying magnetic surveys to prospecting seafloor resources and probing subseafloor structures.

#### 1. Introduction

Mid-ocean ridge basalt (MORB) acquires a thermoremanent magnetization (TRM) upon its eruption and subsequent cooling, generating seafloor magnetism (Gee & Kent, 2007). This TRM, however, is commonly modified when the primary magnetic mineral in MORB—titanomagnetite (Fe<sub>3-x</sub>Ti<sub>x</sub>O<sub>4</sub>) with titanium content (x value) of ~0.6 (TM60; Petersen et al., 1979)—suffers various physicochemical alterations after lava emplacement. Maghemitization (also referred to as low-temperature oxidation) of the primary TM60 at suboceanic conditions has been studied extensively. Oxidation of Fe<sup>2+</sup> to Fe<sup>3+</sup> produces vacancies and cation reordering in the inverse spinel structure of TM60 (Petersen et al., 1979; Xu et al., 1997), replacing the original TRM with a chemical remanent magnetization (CRM; Almeida et al., 2014; Özdemir & Dunlop, 1985). Extremely high oxidation states can even produce self-reversed magnetization (Doubrovine & Tarduno, 2004, 2006). Moreover, maghemitization is regarded as a possible explanation for the long-term variations of seafloor magnetization—a sharp decrease

WANG ET AL. 1 of 17



Writing – original draft: Shishun Wang Writing – review & editing: Shishun Wang, Liao Chang, Chunhui Tao, Dario Bilardello, Long Liu, Tao Wu from 0-20 Ma followed by a gradual increase up to 120 Ma (Bleil & Petersen, 1983; Matzka et al., 2003; Zhou et al., 2001).

In addition to maghemitization, hydrothermal alteration of magnetic minerals is also recognized in MORB (e.g., Dekkers et al., 2014; Shau et al., 2000). Seafloor hydrothermal processes are distinguished as high-temperature vent flows (250–400°C) and low-temperature diffuse flows (<250°C), corresponding to heat sources deriving from axial magma chambers and conductive cooling of the oceanic lithosphere, respectively (Alt, 1995). Diffuse flows are widely distributed in the oceanic crust. Their effects on seafloor magnetism are thought to be similar to maghemitization (Petersen et al., 1979). High-temperature vent flows are more concentrated along mid-ocean ridges and back-arc spreading centers (Beaulieu & Szafranski, 2020). They are catastrophic to the magnetization of MORB as they alter TM60 into nonmagnetic minerals such as chlorite and sphene (e.g., Ade-Hall et al., 1971; Oliva-Urcia et al., 2011), producing prominent negative magnetic anomalies (e.g., Szitkar et al., 2014; M. A. Tivey & Johnson, 2002). Although magnetic surveys have been successfully applied in probing hydrothermal fields (e.g., Galley et al., 2020), the detailed transformation path of TM60 into alteration products and their effects on magnetic properties remain to be elucidated.

Based on multi-scale electron microscopic analyses, S. Wang et al. (2020) recently documented a detailed hydrothermal alteration pathway where titanomagnetites are dissolved by hydrothermal chloritization and brecciation progressively, and nano-scale titanomagnetite inclusions are consumed faster and earlier than the micron-scale titanomagnetite dendrites. They also found that the Ti content (x) drops from  $0.54 \pm 0.05$  for primary titanomagnetite in MORB to  $0.08 \pm 0.02$  for titanomagnetite residues in partially chloritized basalts (S. Wang et al., 2020), indicating possible second-order reactions in addition to the overall titanomagnetite dissolution. However, microscopic analyses are inefficient in recognizing these subtle interactions between magnetic minerals and hydrothermal fluids due to the low concentrations of magnetic minerals in hydrothermally-altered MORB (S. Wang et al., 2020). In this study, the magnetomineralogy of hydrothermally-altered MORB is quantified through comprehensive rock magnetic analyses. Magnetic properties of fresh and hydrothermally-altered MORBs are compared to identify key rock magnetic fingerprints associated with seafloor high-temperature hydrothermal alteration. Integrating with the electron microscopic analyses, a schematic model is proposed to decode the effect of high-temperature hydrothermal processes on magnetic mineral assemblages within MORB, which is critical for understanding seafloor magnetism.

# 2. Materials and Methods

# 2.1. Samples

Fresh and hydrothermally-altered MORBs were dredged along the very-slow-spreading Southwest Indian Ridge (SWIR; 14–16 mm yr<sup>-1</sup> full spreading rate; Dick et al., 2003) near Longqi and Yuhuang hydrothermal fields (Figure 1; Liao et al., 2018; Tao et al., 2012, 2020) using a television-guided grab. Dredging sites show good within-site homogeneity except for sites in hydrothermal fields where rocks of mixed alteration degrees were found. Multiple samples were therefore obtained from different dredged pieces for sites in hydrothermal fields. The studied samples include 41 fresh basalts, 23 chloritized basalts, and 8 chloritized basaltic breccias, which represent a progressive hydrothermal alteration pathway as described in S. Wang et al. (2020). Chloritized basalts and chloritized basaltic breccias are referred to as altered basalts. Chloritized basalts are further divided into partially and fully chloritized basalts depending on whether the original basaltic textures are preserved or not (S. Wang et al., 2020). In the following context, rock magnetic results are discussed according to their lithology classifications (i.e., fresh basalts, partially chloritized basalts, fully chloritized basalts, and chloritized basaltic breccias). Three chips of ~1-cm³ with the same orientation were cut as sister specimens from each sample using a diamond saw, avoiding the weathered coats. Rock powders were also prepared using a ceramic mortar.

# 2.2. Rock Magnetic Measurements

Alternating-field (AF) and thermal demagnetization (TD) were conducted in a magnetically shielded room at the Paleomagnetism Laboratory, Peking University (PKU). Measurements were performed on a 2G-755 cryogenic superconducting rock magnetometer equipped with an automatic sample handling system. For AF, specimens were enclosed in 8-cm³ plastic cubes and immobilized with cotton. AF was imparted in 2-mT steps (0–40 mT) and 5-mT steps (40–120 mT) by in-line AF coils attached to the magnetometer. For TD, specimens were enclosed

WANG ET AL. 2 of 17

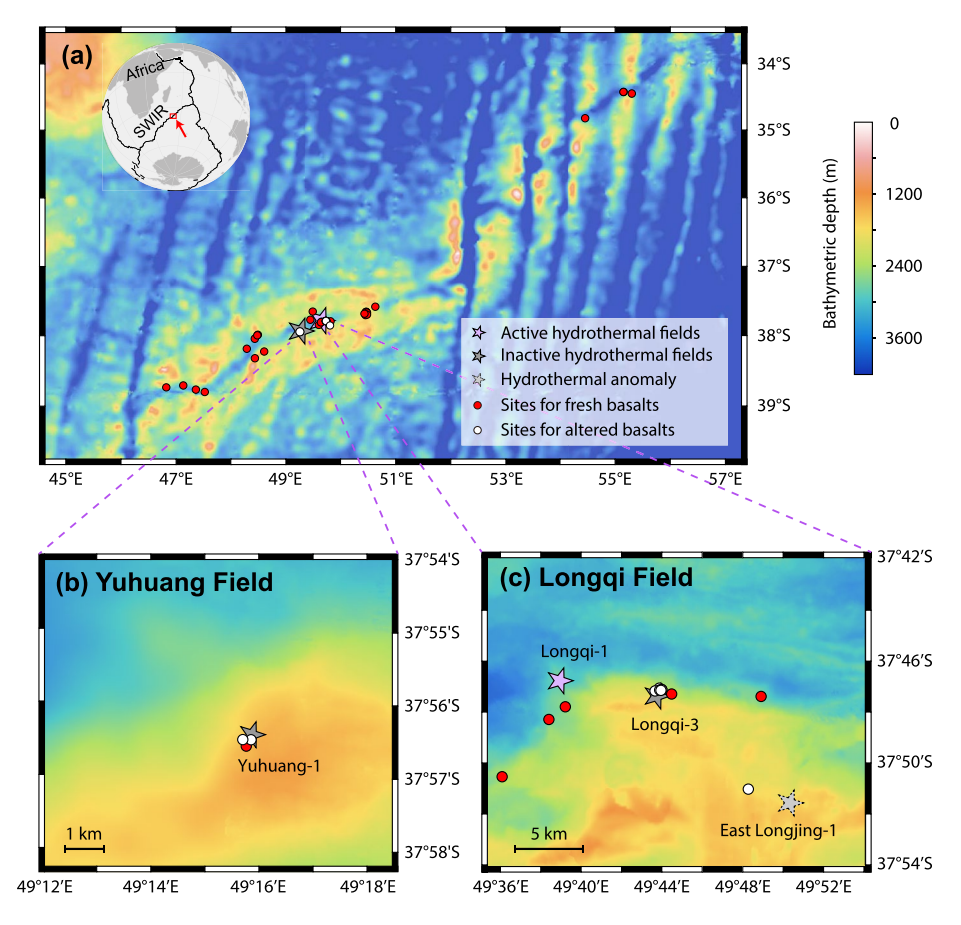


**Figure 1.** Bathymetric maps showing the sites for dredged samples and hydrothermal fields. (a) Bathymetric map with dredging sites and Longqi and Yuhuang hydrothermal fields indicated. The inset provides a global picture of the study area. (b) Yuhuang field zoom-in. Samples were dredged from the southwest sulfide area of the Yuhuang-1 inactive hydrothermal field (Liao et al., 2018). (c) Longqi field zoom-in. Longqi-1 is an active hydrothermal field while Longqi-3 is an inactive one (Tao et al., 2020). East Longjing-1 indicates an area with a hydrothermal anomaly (Tao et al., 2020).

in 8-cm<sup>3</sup> ceramic cubes and immobilized with silica wool. Specimens were heated in air in 25°C steps from 50 to 650°C using an ASC TD-48 thermal demagnetization device. The residual magnetic field in the magnetometer and the TD device is below  $\sim$ 50 nT. The magnetic moment of holder and 8-cm<sup>3</sup> plastic/ceramic cubes were  $\sim$ 10<sup>-11</sup> Am<sup>2</sup>.

Hysteresis loops were measured using a Princeton MicroMag 3900 vibrating sample magnetometer (VSM) at the Institute of Geophysics, China Earthquake Administration in Beijing. 1 and 0.5 T saturation fields were used for fresh and altered basalts, respectively. Coercivity ( $B_c$ ), saturation magnetization ( $M_s$ ), and saturation remanent magnetization ( $M_r$ ) were obtained after paramagnetic corrections using the HystLab program (Paterson et al., 2018). Isothermal remanent magnetization (IRM) acquisition curves for fresh basalts were acquired by measuring 80 logarithmically distributed points from 0.1 mT to 1 T using the VSM. For magnetically weak altered basalts, the IRM was imparted on an ASC impulse magnetizer and measured on the 2G-755 magnetometer at PKU. A total of 60 data points were acquired in a logarithmical distribution from 1 mT to 2.5 T. Partially chloritized basalts were also measured on the VSM to check if there are any biases in impulse-magnetizer-imparted IRMs. IRM components were defined using the skewed generalized Gaussian function (Egli, 2003). IRM component unmixing was performed using the web application MAX Unmix (Maxbauer et al., 2016). First-order reversal curves (FORC; e.g., Roberts et al., 2000) were measured for all 41 fresh basalts using the same parameters: 250 mT  $B_c$ ,  $\pm 50$  mT  $B_u$ , and 800 mT saturation field, for a total of 130 FORCs per specimen. FORC data were processed using the software Forcot (Berndt & Chang, 2019).

WANG ET AL. 3 of 17



Temperature-dependent magnetic susceptibility was measured in argon for all samples in heating-cooling cycles between 50 and 700°C with a rate of ~13.7°C/min using an AGICO Kappabridge (model MFK-1FA) at PKU. The applied field was 200 A/m and the operating frequency was 976 Hz. Low-temperature alternating current (AC) susceptibility was measured on selected samples from 10 to 300 K in a 5 K step and a 5 K/min rate with 238.7 A/m applied field and operating frequencies of 1, 10, and 100 Hz. For low-temperature magnetic remanence measurements, specimens were cooled from 300 to 10 K in a 2.5 T field (FC). Zero-field-cooled (ZFC) curves, instead, were acquired by cooling in zero-field and imparting a low-temperature 2.5 T saturation IRM (SIRM) at 10 K. Remanence was then measured in a 2.5 K step with a 5 K/min rate from 10 to 300 K in zero field. Subsequently, samples were imparted a room-temperature SIRM in a 2.5 T field, and remanence was then measured in zero field at a 2.5 K step through a 300 K-10 K - 300 K low-temperature cycle (LTC) with a 5 K/min rate. All low-temperature measurements were performed on a Quantum Design Magnetic Property Measurement System (MPMS) either at the Institute of Rock Magnetism (model MPMS-XL), University of Minnesota, or at the Institute of Geomechanics (model MPMS3), Chinese Geological Survey in Beijing.

#### 2.3. Electron Microscopic Analyses

Microscopic analyses were performed on carbon-coated rock thin sections of typical samples using an FEI QUANTA-650FEG field-emission scanning electron microscope (SEM) at PKU. Backscattered electron (BSE) image and X-ray energy dispersive spectrometry (EDS) were obtained with 10–15 kV accelerating voltage and 10 mm working distance.

#### 3. Results

#### 3.1. Demagnetization of the Natural Remanent Magnetization (NRM)

Fresh basalts have stable NRMs that decrease sharply between 10 and 40 mT AF or 100 and 250°C TD and more gradually between 40 and 120 mT AF or 250 and 550°C TD (Figures 2a and 2b). Some fresh basalt samples have a plateau in the temperature-dependent magnetization curve at 250–425°C (Figure 2d), but no obvious peculiarity is observed in the corresponding magnetization-AF curves (Figure 2c). This is likely caused by partially self-reversed magnetization during heating, which indicates partial oxidation of samples before heating (Pan et al., 2006; Text S1 and Figure S1 in Supporting Information S1). No stable NRM was preserved in fully-altered chloritized basaltic breccias (Figures 2g and 2h). The demagnetization behavior of chloritized basalts depends on the alteration degree: fully chloritized samples behave like chloritized basaltic breccias, whereas for samples with slight to intermediate chloritization degree, the NRM is retained but is unblocked by ~30 mT AF or ~300°C heating (Figures 2e and 2f). The highest measured fluid temperature at the Longqi hydrothermal field is 379°C (Tao et al., 2012), and thus the remanence recorded by chloritized basalts is likely a CRM acquired during hydrothermal alteration.

#### 3.2. IRM Acquisition Curves and Unmixing

The IRM acquisition curves of fresh basalts can be unmixed using two components (Figures 3a and 3b). The lower coercivity components (blue) have mean remanence coercivity ( $B_h$ ) values of 25.1–56.2 mT and dispersion parameters (DP) around 0.25, while the mean  $B_h$  and DP for higher coercivity components (violet) are around 44.7–346.7 mT and 0.30, respectively. Altered basalts show large variability—the main peak can be unmixed by either one or two components with an additional high-field (green) component (Figures 3c–3f). The green component typically has  $B_h$  values over 316–1000 mT with some samples unsaturated in a 2.5-T field. No significant discrepancies were observed between VSM and impulse-magnetizer-imparted IRMs (Figure S3 in Supporting Information S1).

K-means cluster analysis was performed to extract statistical information from certain properties for all unmixed IRM components. Four fitted IRM parameters (i.e.,  $B_h$ , DP, proportion, and skewness; Egli, 2003) were considered as four data dimensions in k-means clustering. To determine the optimal cluster numbers used for fresh and altered basalts, the total Euclidean distance between data points and their clustering centroids was plotted against the number of clusters after averaging 100 runs (Figure 3g). The "elbows" indicate 2 clusters for the fresh basalts and either 3 or 4 clusters for the altered basalts. Considering the IRM unmixing results, 3 clusters were chosen

WANG ET AL. 4 of 17

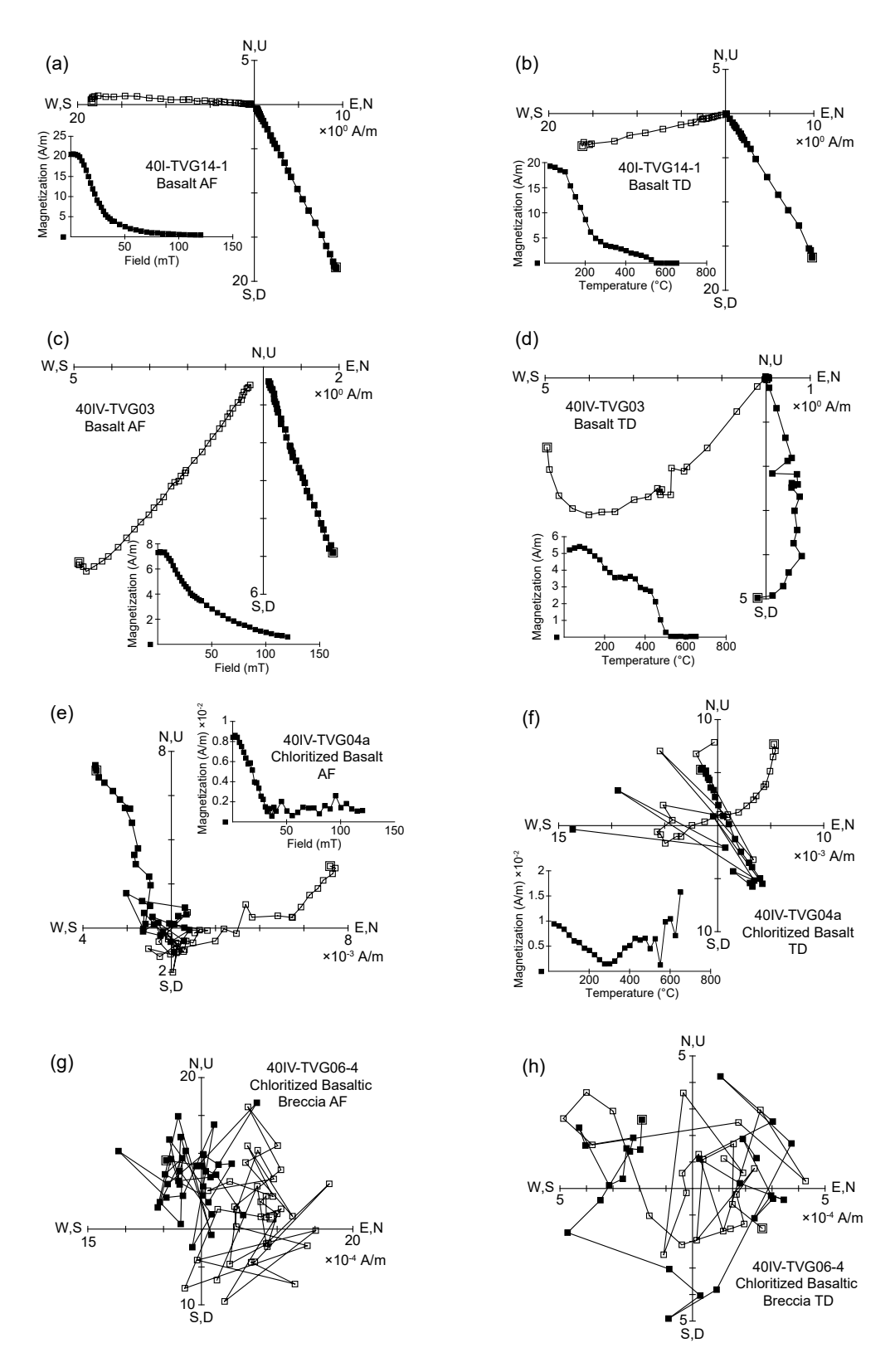


Figure 2.

WANG ET AL. 5 of 17



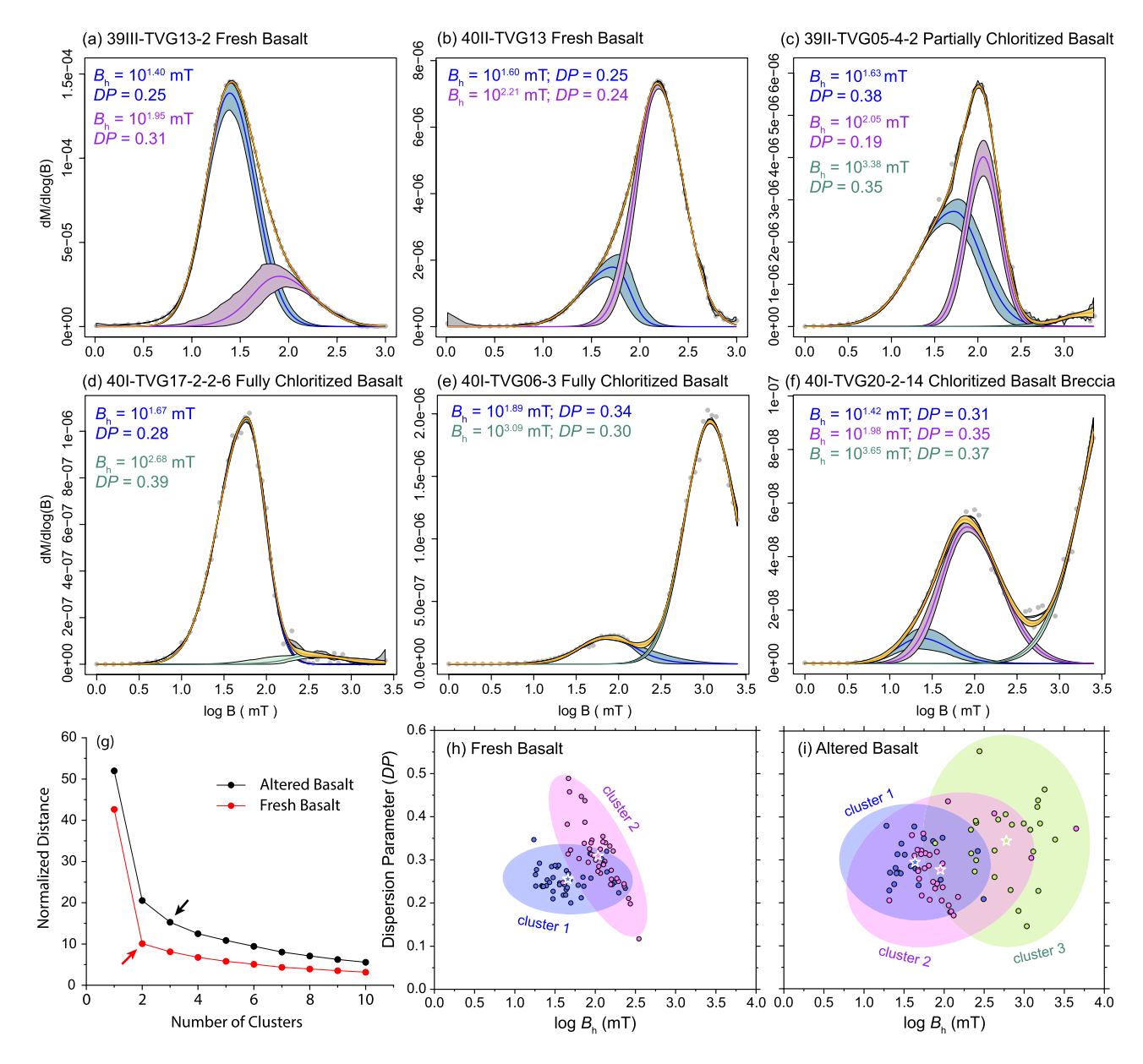


Figure 3. Unmixing of isothermal remanent magnetization (IRM) acquisition curves and k-means clustering analysis of parameters for the unmixed components. (a–f) Unmixed IRM acquisition curve of representative fresh basalts (a–b), partially chloritized basalts (c), fully chloritized basalts (d–e), and chloritized basaltic breccia (f) samples. Mean remanence coercivity ( $B_h$ ) and dispersion parameter (DP) of unmixed components are indicated. Shaded bands are 95% confidence level. (g–i) K-means cluster analyses of fitted IRM parameters for all unmixed components. (g) Elbow method with arrows showing the optimal number of clusters for fresh and altered basalts. (h–i) DP plots with log  $B_h$  from results of k-means cluster analyses. Cluster centroids are given by white-edged stars with data in Table 1. The shaded areas are the 95% confidence ellipses of clusters.

for the altered basalts. The final results were determined from 20 replicates to avoid non-uniqueness introduced by random initialization, which assures reproducibility of the clustering results. Figures 3h and 3i show the clustering results of fresh and altered basalts reducing to  $B_h$ -DP dimensions, and Table 1 reports the clustering

Figure 2. Natural remanent magnetization demagnetization for typical samples of different lithologies and alterations. Stepwise alternating-field (AF) and thermal demagnetization (TD) plots were obtained from sister specimens of fresh basalt samples 40I-TVG14-1 (a–b) and 39I-TVG03 (c–d), chloritized basalt sample 40IV-TVG04a (e–f), and chloritized basaltic breccia sample 40IV-TVG06-4 (g–h). Open and solid squares indicate vertical and horizontal plane projections, respectively. Insets show magnetization as a function of increased AF or temperature. Note that the orientations for all dredged samples were determined during sample preparation. The small inconsistency in directions among sister specimens is due to the disturbance when sealing the specimen fragments into plastic or ceramic cubes. Demagnetization plots were produced using the PuffinPlot program (Lurcock & Wilson, 2012).

WANG ET AL. 6 of 17



Table 1           Clustering Centroids for IRM Components From k-Means Cluster Analyses								
Lithology group	Cluster	$B_{\rm h}({ m mT})$	DP	P	S			
Fresh Basalt	Cluster 1 (blue)	$10^{1.660}$	0.255	0.909	0.995			
	Cluster 2 (violet)	$10^{2.035}$	0.309	0.211	1.028			
Altered Basalt	Cluster 1 (blue)	$10^{1.637}$	0.295	0.348	0.947			
	Cluster 2 (violet)	$10^{1.955}$	0.277	0.905	0.966			

Note.  $B_h$ , mean remanence coercivity; DP, dispersion parameters; P, proportions; S, skewness.

Cluster 3 (green)

 $10^{2.778}$ 

0.344

0.164

1.270

centroids. The blue (low coercivity) and violet (high coercivity) components of the fresh basalts form two partially overlapping clusters (Figure 3h). The dispersion parameter of the violet components decreases with increasing remanence coercivity, producing an elongated pattern. Altered basalts are distinguished from fresh basalts by the presence of high-field (green) components (Figure 3i). Cluster 1 and 2 in altered basalts completely overlap and have more scattered clustering than the fresh basalts resulting from modifications of the magnetic mineralogy by hydrothermal alteration.

## 3.3. High-Temperature Dependent Magnetic Susceptibility ( $\chi$ -T)

The  $\chi$ -T curves of fresh basalts can be resolved into two predominant components with Curie temperatures lower than 200°C (Figure 4a) and around 350–400°C (Figure 4b), corresponding to different groups of titanomagnetite. A

combination of these two components is found in most fresh basalt samples (Figure 4c). The smaller hump at ~400–600°C is consistent with inversion of oxidized titanomagnetite (Krása & Matzka, 2007). The irreversibility of the heating/cooling curves is likely caused by the inversion products and ordering state changes during heating (Harrison & Putnis, 1999). For partially chloritized basalts, magnetic susceptibility increased during heating with a bump between ~150 and 350°C (Figure 4d). The bump results from the annealing of stresses of the oxidized (titano) magnetites (Bilardello, 2020) and is typical for alteration-related samples (e.g., Bowles et al., 2020; Kontny & Grothaus, 2017; Krása & Herrero-Bervera, 2005). Oxidized titanomagnetite also existed in fully chloritized basalts (Figure 4e): a susceptibility drop was observed in the heating curve around 350°C, but unlike data for fresh basalts (i.e., Figure 4b), it was completely unrecoverable in the cooling curve. Oxidized titanomagnetite became stoichiometric magnetite after being heated to 700°C. Fully chloritized samples with scarce magnetic minerals have low susceptibilities (Figure 4f). Heating results in a peak at around 500–600°C, amplified in the cooling curve, indicating that magnetite was produced from chlorite or other altered minerals (e.g., Just & Kontny, 2012).

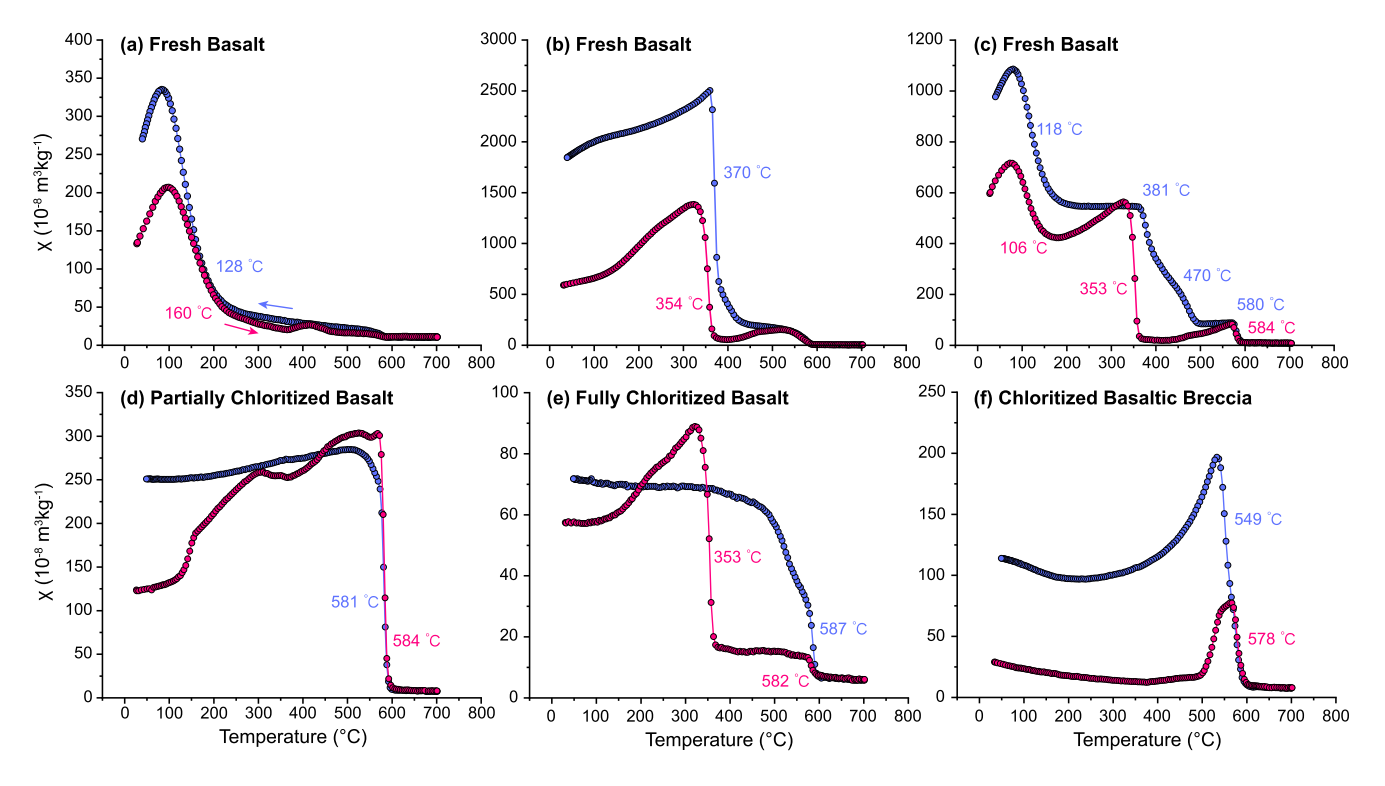


Figure 4. High-temperature dependent magnetic susceptibility ( $\chi$ -T) of representative samples: fresh basalt samples 39I-TVG02 (a), 39I-TVG08 (b), and 40II-TVG11 (c), partially chloritized basalt sample 39II-TVG05-2-9 (d), fully chloritized basalt sample 40I-TVG22-1-2 (e), and chloritized basaltic breccia sample 40I-TVG20-2-14 (f). Heating and cooling curves are presented in red and blue, respectively. The marked Curie temperatures were estimated from slope minimums at susceptibility drops. The corresponding derivative curves can be found in Figure S4 in Supporting Information S1.

WANG ET AL. 7 of 17



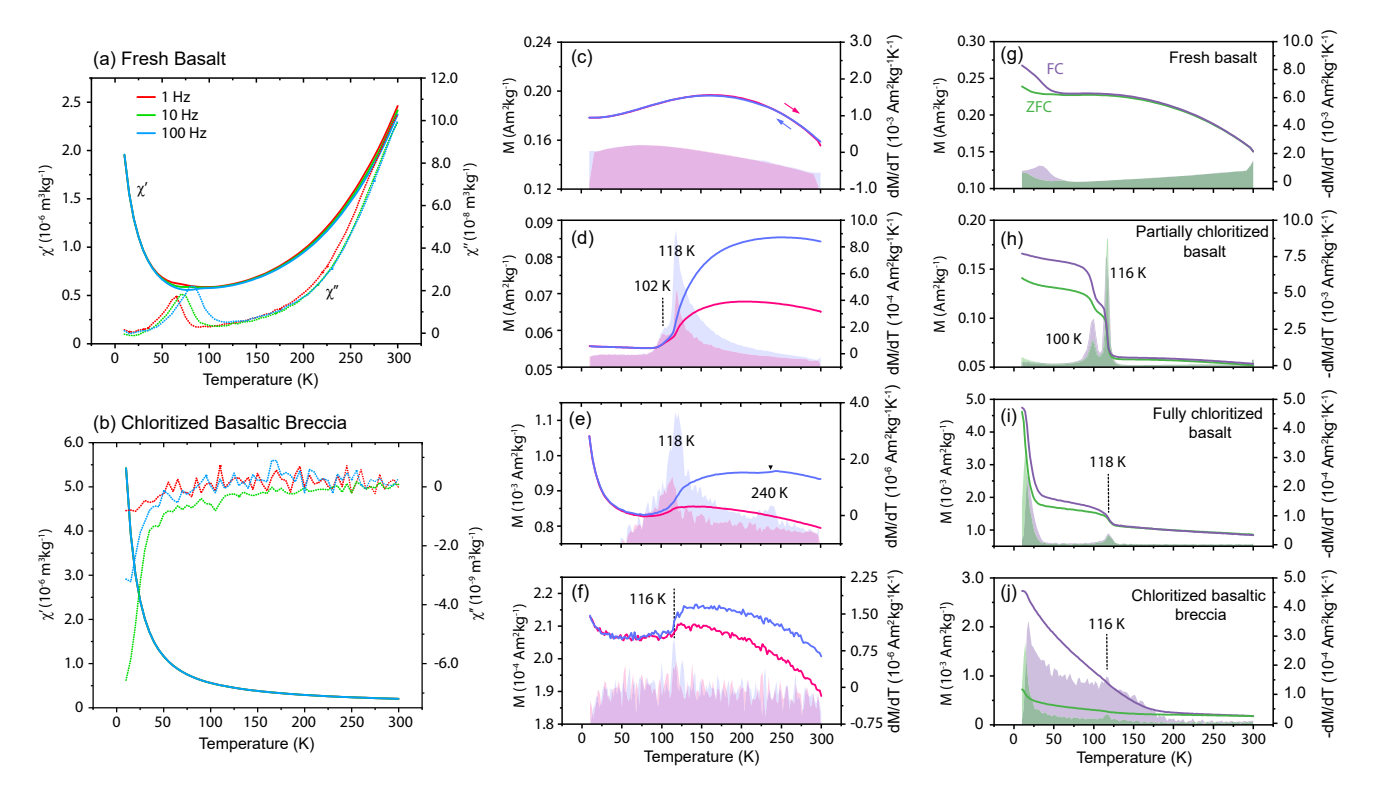


Figure 5. Low-temperature magnetic property data. (a) and (b) Alternating current susceptibility measured on a fresh basalt sample 40IV-TVG18 (a) and a fully-altered chloritized basaltic breccia sample 40IV-TVG06-2 (b). Solid and dotted colored lines are in-phase ( $\chi'$ ) and out-of-phase ( $\chi''$ ) susceptibilities measured with 1, 10, and 100 Hz frequencies. (c)–(f) Low-temperature cycling (LTC) of a room-temperature saturation isothermal remanent magnetization (SIRM) measured on a fresh basalt sample 39I-TVG02 (c), a partially chloritized basalt sample 39I-TVG05-4-2 (d), a fully chloritized sample 40I-TVG22-1-1 (e), and a chloritized basaltic breccia sample 40IV-TVG06-2 (f). (g)–(j) Corresponding field-cooled (FC) and zero-field-cooled (ZFC) heating curves of samples shown in (c)–(f). Chloritized basaltic breccia sample has noisy data because of its low magnetization. The terrains in the background of (c)–(j) are the first derivatives and are related to individual curves with same colors. The magnetite Verwey transition temperatures are indicated. Blue and red arrows indicate cooling and heating, respectively. The black triangle in (e) marks the hematite Morin transition.

# 3.4. Low-Temperature Magnetic Measurements

Fresh and altered basalts both have significant paramagnetic fractions contributing to AC susceptibility as a strong hyperbolic decrease of in-phase susceptibility with increasing temperature below ~50 K (Figures 5a, 5b, and S5 in Supporting Information S1). Above ~50 K, temperature-dependent susceptibility decrease for altered basalts still follows the Curie-Weiss law (Figure 5b), while fresh basalts have ferromagnetic features superimposed on the paramagnetic signal (Figure 5a). At 50–100 K, fresh basalts exhibited frequency-dependent in-phase and out-of-phase susceptibilities, which are likely caused by thermally activated long-range electron hopping of titanomagnetite, associated with domain wall relaxation (Church et al., 2011; Moskowitz et al., 1998). Above 100 K, both in-phase and out-of-phase susceptibilities increase parabolically and peak above 300 K, indicating the presence of single-domain (SD) particles with blocking temperature above room temperature (Bowles et al., 2009; Till et al., 2011).

Fresh basalts have reversible LTC curves with a hump between 150 and 200 K (Figure 5c) probably due to magnetic anisotropy variations of Ti-rich titanomagnetites (e.g., Kąkol et al., 1991). ZFC and FC curves converge at  $\sim$ 50 K (Figure 5g), which is consistent with the thermal dependence of anisotropy and magnetostriction constants for Ti-rich titanomagnetites (Moskowitz et al., 1998). Altered basalts show magnetite Verwey transitions (Verwey, 1939) in low-temperature remanence curves compared to fresh basalts. Fully chloritized basalts and chloritized basaltic breccias have Verwey transition temperatures ( $T_v$ ) of 115–120 K (Figures 5e, 5f, 5i, and 5j), corresponding to near stoichiometric magnetite. Partially chloritized basalts present characteristic dual Verwey transitions at  $\sim$ 100 K and 115–120 K (Figures 5d and 5h). Electron microscopic analyses reveal that titanomagnetites generally occur as micron-scale alteration residues in partially chloritized basalts (Figure 6a) and have reduced titanium contents compared to fresh basalts (Figures 6f1; S. Wang et al., 2020). Although primary

WANG ET AL. 8 of 17

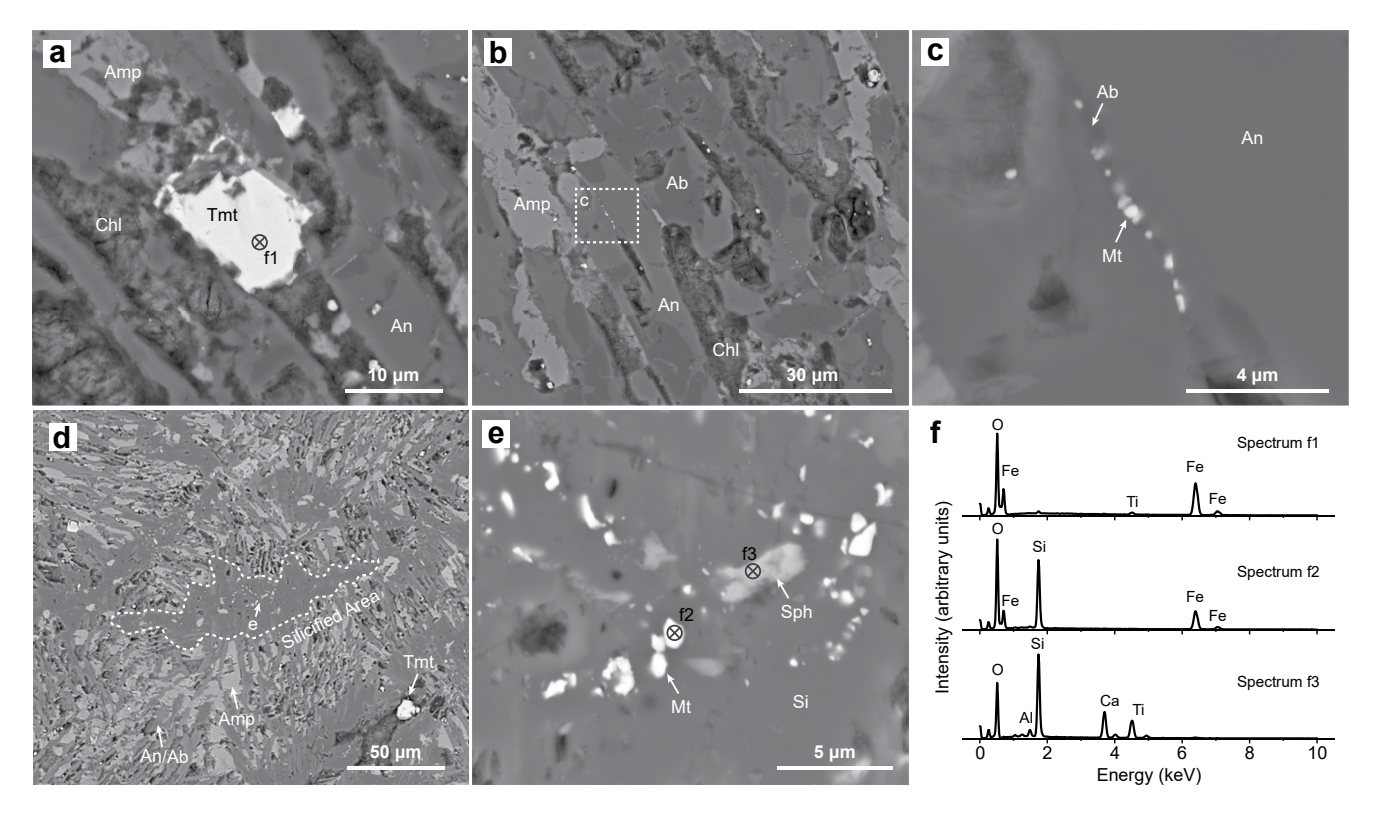


**Figure 6.** Scanning electron microscopic analyses of partially chloritized basalts. Backscattered electron (BSE) images (a–e) and energy dispersive spectra (EDS; f) were obtained from samples 39II-TVG05-4-2 (a–c) and 40I-TVG17-1-2 (d–e). EDS was acquired at positions marked by the circle with cross. Note that the Si signal in spectrum f2 is from the silica matrix. Mineral abbreviations are: Ab = albite, Amp = amphibole, An = anorthite, Chl = chlorite, Mt = magnetite, Si = silica, Sph = sphene, and Tmt = titanomagnetite.

nanoscale titanomagnetite inclusions were dissolved during initial chloritization (S. Wang et al., 2020), a small group of magnetite inclusions was produced during alteration. They typically have grain sizes of  $<1-2~\mu m$  and are embedded in either albitized plagioclases (Figures 6b and 6c) or silicified areas (Figures 6d, 6e, and 6f2) of hydrothermal origin (Alt, 1995). Note that these secondary magnetite inclusions often coexist with sphene crystals (Figures 6e and 6f3). The presence of both low-titanium titanomagnetite alteration residues and hydrothermally-produced magnetite inclusions in partially chloritized basalt explains the dual Verwey transitions in low-temperature magnetic measurements (Figures 5d and 5h) and corroborates the high-temperature susceptibility results (Figure 4d).

In addition to magnetite, other magnetic minerals are also evident in low-temperature remanence measurements for altered basalts. The hematite Morin transition (Morin, 1950; Özdemir et al., 2008) can be observed at around 230–250 K (Figure 5e). FC and ZFC curves have large separations and converge at a temperature beyond  $T_{\rm v}$  (Figure 5j), indicating contributions from goethite (Liu et al., 2006). The presence of hematite and goethite is confirmed by the 2.5 T unsaturated high-field component in the IRM acquisition curve unmixing (Figures 3e and 3f).

#### 3.5. Hysteresis Properties

Fresh basalts exhibit an exponential trend in the  $M_{\rm rs}/M_{\rm s}$  (squareness)— $B_{\rm c}$  plot with a maximum squareness of 0.67 (Figure 7a). The exponential trend represents variations in crystallization: toward the origin (i.e., low  $B_{\rm c}$  and  $M_{\rm rs}/M_{\rm s}$  values), basalts are dominated by complex-shaped micron-scale titanomagnetite dendrites; to the other end, basalts show typical quenching textures with dominance of nano-scale Fe-Ti oxides (Figures 7e-7g and S7 in Supporting Information S1). High-resolution transmission electron microscopic (TEM) analyses have confirmed that these Fe-Ti oxides are titanomagnetite (S. Wang et al., 2020). Altered basalts have a "lowered" linear trend caused by low-Ti titanomagnetite or magnetite produced by hydrothermal alteration (Figure 7a; D. Wang & Van der Voo, 2004). In FORC diagrams, MORBs with abundant micron-scale titanomagnetites tend to have coercivity

WANG ET AL. 9 of 17



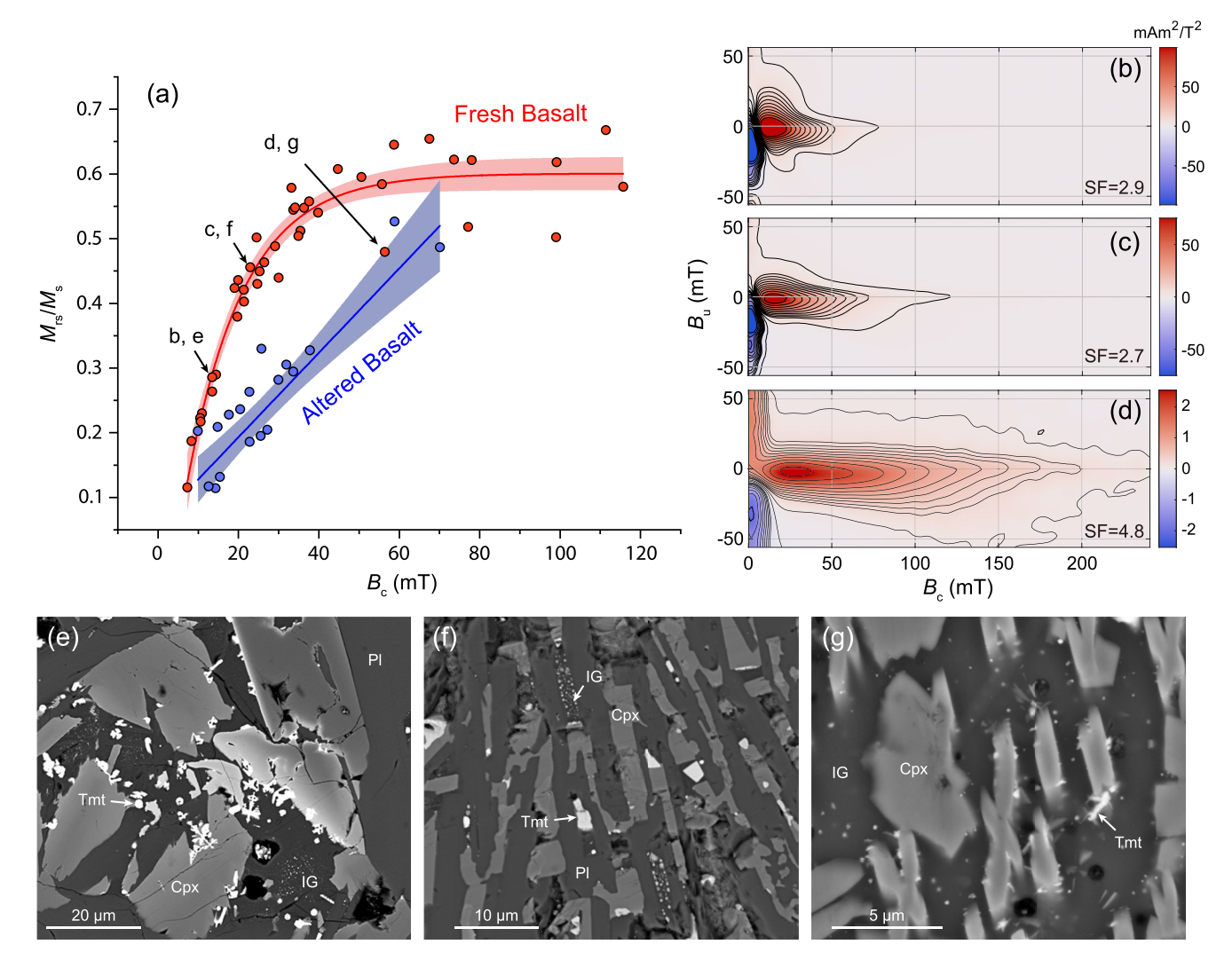


Figure 7. Hysteresis signatures and microstructures of fresh MORBs. (a) Saturation remanent magnetization  $(M_R)$  to saturation magnetization  $(M_R)$  ratio plots with coercivity  $(B_c)$ . Fully altered paramagnetic samples are not shown. Data for fresh basalts were exponentially fitted with  $M_R/M_s = A\exp(R_0B_c) + y_0$ , where  $A = -0.793 \pm 0.062$ ,  $R_0 = -0.0698 \pm 0.0072$ , and  $y_0 = -0.601 \pm 0.013$ . Altered basalts were linearly fitted with  $M_R/M_s = kB_c + b$ , where  $k = 0.00652 \pm 0.00074$  and  $b = 0.0801 \pm 0.0230$ . Shadowed bands represent the 95% confidence. (b)–(d) First-order reversal curves (FORC) for samples indicated by arrows in (a). Smoothing factors (SF) were automatically optimized by Forcot software (Berndt & Chang, 2019). (e)–(g) Corresponding backscattered electron (BSE) overviews of the same samples in (b)–(d) show typical titanomagnetite microstructures. Mineral abbreviations are: Tmt = titanomagnetite, Cpx = clinopyroxene, Pl = plagioclase, and IG = interstitial glasses.

distributions mostly within 50–100 mT (Figures 7b and 7c), while those dominated by nano-scale titanomagnetites have dispersed coercivity distributions over 200 mT (Figure 7d). Vertically distributed inverted trapezoidal contours are observed in all measured FORC diagrams, indicating the dominance of interacting SD particles (Roberts et al., 2014). The negative regions at the bottom left and the small ridges at  $B_u = 0$  correspond to uniaxial noninteracting SD grains (Newell, 2005). Contributions from vortex state particles and/or grains with contrasting magnetic states are evident by vertically extruded lobes (Lascu et al., 2018; Roberts et al., 2014, 2017) and are more prominent in samples with complex-shaped titanomagnetite dendrites (Figures 7b and 7c).

# 4. Discussions

#### 4.1. Hysteresis Signatures of Nano- and Micron-Scale Titanomagnetites in Fresh MORBs

Before evaluating the magnetic signatures associated with hydrothermal alteration, it is important to understand the natural variability of magnetic properties for fresh MORBs. Micron-scale titanomagnetites were in metastable

WANG ET AL. 10 of 17



Lithology	Type of NRM	IRM unmixing <sup>a</sup>	χ-T curve	Low-temperature transitions
Fresh Basalt	TRM (41/41) <sup>b</sup>	Two components (41/41)	$T_{c1}$ <200°C $T_{c2}$ = 350–400°C (39/41)	No phase transition (6/6)
Partially Chloritized Basalt	CRM (21/31)	Additional high-field component (25/31)	Maghemite bump ∼150–350°C (4/6)	Dual Verwey transition $T_{v1} = \sim 100 \text{ K}$ $T_{v2} = 115-120 \text{ K}$ $(3/4)$
Fully Chloritized Basalt & Chloritized Basaltic Breccia	No Remanence (10/31)		Heating produces magnetite (23/25)	Verwey transition $T_v = 115-120 \text{ K}$ Evidence for hematite and goethit (5/5)

Note. CRM, chemical remanent magnetization; IRM, isothermal remanent magnetization; NRM, natural remanent magnetization; TRM, thermoremanent magnetization;  $\chi$ -T, temperature dependence of magnetic susceptibility.  $T_c$  and  $T_v$  are Curie temperature and magnetite Verwey transition temperature, respectively.

aSee Table 1 for statistical information. bThe numbers in parentheses (m/n) indicate m of n measured samples with such signature.

equilibrium with the initial melts, which is evident by the brightness gradient in Figure 7e where the micron-scale particles adhere to and take up iron from clinopyroxene (e.g., Pontesilli et al., 2019). Nano-scale titanomagnetites crystallized posterior to micron-scale ones through quenching of a differentiated melt (Zhou et al., 2000, 2001). Vertically-extended lobes and positive ridges along  $+B_u$  axis in FORC diagrams (Figures 7b–7d) together with frequency-dependent AC susceptibility around 50–100 K (Figure 5a) indicate that the  $\sim$ 5–10  $\mu$ m micron-scale titanomagnetites are in vortex to multi-domain states, which is consistent with the observations by Shaar and Feinberg (2013). The nano-scale titanomagnetites have wide grain size distributions from  $\sim$ 50 to >150 nm (S. Wang et al., 2020; Figure S7 in Supporting Information S1), corresponding to SD to vortex states (e.g., Nikolaisen et al., 2020). Nano-scale titanomagnetites generally have high and wide coercivity distributions, but their signals are often blanketed by micron-scale titanomagnetites in MORBs. This was confirmed by chemically extracted nano-scale titanomagnetites prepared for deposition experiments: coercivity distribution expands toward high fields after dissolving the micron-scale titanomagnetites by hydrochloric acid (Chang et al., 2021).

The exponential trend of MORBs in the squareness versus coercivity plot represents the relative contributions of micron- and nano-scale titanomagnetites. According to the modeling results of Tauxe et al. (2002), coercivity of ~40 mT and squareness of ~0.5 mark the turning point from vortex states into SD regime. The ~0.6 squareness is interpreted to reflect particles with "complicated shapes" by Tauxe et al. (2002), but in this case, it is likely a consequence of undersaturation (Fabian, 2006) as the hysteresis loops of quenched samples merge just below 1 T field (Figure S6 in Supporting Information S1). The ideal convergence point of squareness should be closer to the uniaxial SD trend of Tauxe et al. (2002). Indeed, the high coercivities of nano-scale titanomagnetites can be caused by shape anisotropies, as K-means clustering of high-coercivity (violet) components for fresh MORBs shows decreasing DP with increasing  $B_h$  (Figure 3h), which is typical for elongated particles with predominant shape anisotropy (e.g., Bai et al., 2021; Chang et al., 2019). Enhanced internal stress during quenching can also be an important factor that keeps coercivity increasing after "saturation" of squareness (Fabian, 2006; Nikolaisen et al., 2020). Overall, the exponential trend verifies the modeling results of Tauxe et al. (2002). As a potential substitute for the Day plot (Roberts et al., 2018), the squareness versus coercivity plot is powerful in distinguishing the relative dominance of nano- and micron-scale titanomagnetite in MORB.

# ${\bf 4.2.} \ \ Magnetic \ Fingerprints \ of \ High-Temperature \ Hydrothermal \ Alteration \ in \ MORB \ and \ Their Implications for \ Tracing \ the \ Alteration \ Process$

Compared to maghemitization of titanomagnetite in MORBs, the recognition of the high-temperature hydrothermal alteration traditionally relies on petrographic analyses, while its magnetic signatures are insufficiently documented. Our study provides a valuable dataset that not only characterizes the magnetic fingerprints of high-temperature hydrothermal alteration but also decodes the complex interactions between magnetic minerals and hydrothermal fluids. Table 2 summarizes the contrasting magnetic properties of MORB and its high-temperature

WANG ET AL.



alteration products. The presence of the magnetite Verwey transition constitutes a major discriminating factor between fresh and hydrothermally-altered MORBs. More fascinatingly, the studied partially chloritized basalts show unique dual Verwey transitions (Table 2; Figure 5) that correspond to the low-Ti micron-scale titanomagnetite residues and hydrothermally-produced magnetite (Figure 6). Considering that these magnetite grains coexist with sphene and titanomagnetite Ti-content decreases during hydrothermal alteration (Figure 6), we hereby propose that hydrothermal alteration of primary titanomagnetite involves second-order exsolution of Fe-rich and Ti-rich phases, superimposed on the hydrothermal dissolution of titanomagnetite (S. Wang et al., 2020).

Although Ti is considered an immobile element due to its conserved concentration during alteration (e.g., Chesworth et al., 1981), it can be reaccommodated into alteration-produced minerals during the hydrothermal breakdown of the host minerals (e.g., Oliva-Urcia et al., 2011; Pochon et al., 2017). TM60 is thermodynamically unstable at hydrothermal temperatures (<400°C) and thus it tends to exsolve into Fe-rich and Ti-rich phases (Nagata, 1961; Petersen et al., 1979). Both Fe-rich and Ti-rich phases should have been dissolved in the hydrothermal fluids (Stefánsson, 2001). Interestingly, we observe that the Fe-rich phase is still preserved as low-Ti titanomagnetite residues, while the Ti-rich phase has been fully replaced by coexisting magnetite and sphene. Understanding the detailed dissolution mechanism is challenging as complex dissolution-precipitation coupling is involved at the mineral-fluid interface (Ruiz-Agudo et al., 2014). One possible explanation from thermodynamic calculations is that Ti-rich phases (e.g., ulvöspinel and ilmenite) are under a more undersaturated state than Fe-rich phases (e.g., low-Ti titanomagnetite and magnetite) in hydrothermal fluids (Stefánsson et al., 2001). The Ti-rich phase was hence preferentially dissolved in hydrothermal fluids becoming Fe(OH)<sub>2</sub>, Fe(OH)<sub>3</sub>, and Ti(OH)<sub>4</sub> (Stefánsson, 2001). Ti(OH)<sub>4</sub> reacted with siliceous hydrothermal fluids and formed sphene (CaTiSiO<sub>5</sub>):

```
Ti(OH)_4 + Ca^{2+} + H_4SiO_4 = CaTiSiO_5 + 3H_2O + 2H^+, (Oliva-Urcia et al., 2011).
```

The Ca<sup>2+</sup> was derived from the albitization of anorthite (Figure 6):

 $CaAl_2Si_2O_8 + 2Na^+ + 4SiO_2(aq) = 2NaAlSi_3O_8 + Ca^{2+}$ , (M. K. Tivey, 2007).

Magnetite is formed through recrystallization of Fe(OH)<sub>2</sub> and Fe(OH)<sub>3</sub>:

 $Fe(OH)_2 + 2Fe(OH)_3 = Fe_3O_4 + 4H_2O$ , (modified from Iwasaki et al., 2012).

Recrystallized magnetite produces the ubiquitous Verwey transition in hydrothermally-altered MORBs. Part of the Fe and Ti in the hydrothermal fluid may have derived from dissolved titanomagnetite and have contributed to magnetite and sphene formation, especially those nano-scale titanomagnetite inclusions firstly consumed during initial chloritization (S. Wang et al., 2020).

To construct a schematic model of magnetomineralogy evolution during hydrothermal alteration, we compare our dredged samples with drill cores from the Trans-Atlantic Geotraverse (TAG) active hydrothermal mound, obtained during Ocean Drilling Program (ODP) Leg 158 (Humphris et al., 1995, 1996). From bottom to top, the internal stockwork of the TAG active mound can be divided into chloritized zone, silicified zone, anhydrite zone, and sulfide zone (Humphris et al., 1995, 1996, Figure 8a). Petrographic and geochemical analyses revealed that chloritized basaltic breccia (CBB) and silicified wallrock breccia (SWB) in chloritized and silicified zones represent a progressive hydrothermal alteration sequence of MORB wallrocks (Honnorez et al., 1998). The SWIR fresh MORBs and CBBs correlate well with the MORB wallrocks and CBBs beneath the TAG mound, enabling a projection of our dredged samples to the TAG mound transection (Figure 8a). A small number of pyrite veins were found in our CBBs (S. Wang et al., 2020), which can be related to their origins from stockwork zones. However, less sulfur is found in our samples compared to TAG drill cores (Humphris et al., 1995, 1996), probably because the dredged sites are not as close to the hydrothermal discharge zones (>100 m; Figure 1). The partially and fully chloritized basalts are regarded as intermediate alteration products in between MORB and CBB based on their petrographic signatures (S. Wang et al., 2020).

The first-order effect of high-temperature seafloor hydrothermal vent alteration is the progressive dissolution of primary titanomagnetites, as indicated by the decreasing abundance of magnetic minerals in Figure 8b. Exsolution is a superimposed second-order process modifying the magnetomineralogy. During initial chloritization, nano-scale titanomagnetite inclusions were consumed while micron-scale titanomagnetite dendrites were modified and became residues. Such modifications involve both exsolution of Fe-rich and Ti-rich phases and dissolution. Titanomagnetite residues are the exsolved Fe-rich phase with a reduced Ti content, while the Ti-rich phase was

WANG ET AL. 12 of 17



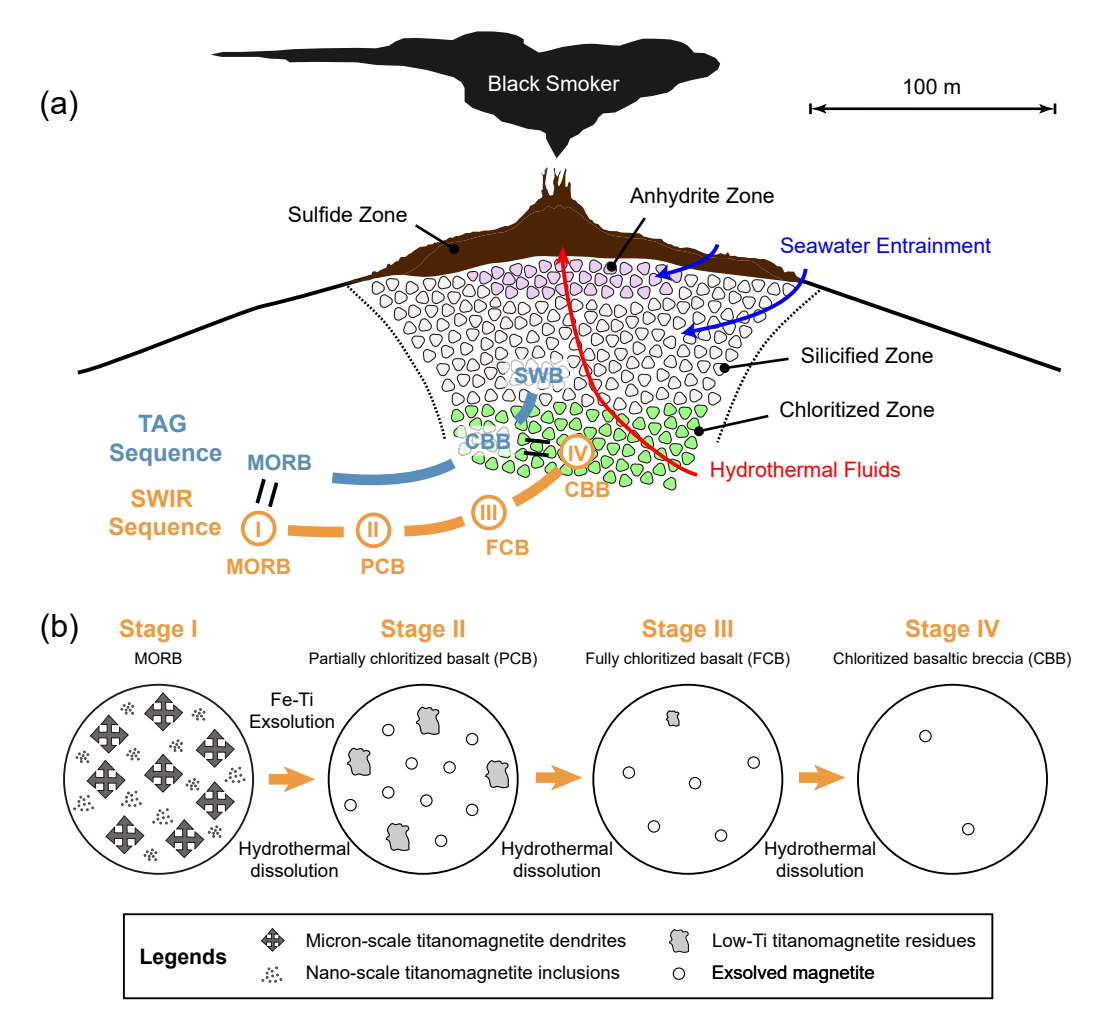


Figure 8. Schematic diagram showing magnetomineralogical variation during high-temperature hydrothermal alteration near seafloor hydrothermal fields. (a) Projection of SWIR dredged samples to the TAG mound transection through lithology correlations. The vent morphology, fluid circulation pattern, and deep structures were sketched from M. K. Tivey (2007). Dotted lines enclose the stockwork, which is divided into chloritized zone, silicified zone, anhydrite zone, and sulfide zone based on the drilling results of Ocean Drilling Program (ODP) Leg 158 (Humphris et al., 1995, 1996). The TAG hydrothermal alteration sequence is from Honnorez et al. (1998), which includes MORB, chloritized basaltic breccias (CBB), and silicified wallrock breccias (SWB). (b) Magnetomineralogical variations of the established SWIR hydrothermal alteration pathway in this study and Wang et al. (2020). Stages I to IV are consistent with the SWIR sequence in (a) and correspond with the lithology of MORB, partially chloritized basalt, fully chloritized basalt, and chloritized basaltic breccias, respectively. Typical magnetic mineral components are indicated.

disseminated in siliceous hydrothermal fluids to form sphene and magnetite, together with the dissolved Fe and Ti from both micron- and nano-scale titanomagnetites. The newly formed magnetite did not make up for the dissolution of primary titanomagnetite. As alteration proceeded, only trace amounts of magnetite or titanomagnetite "survivors" were found in fully-altered products. Not shown in this model are the hematite and goethite found in altered basalts (Figures 3 and 5). According to investigations of the extinct mounds at the TAG field, hematite and goethite can be produced by oxidizing flows far posterior to the high-temperature hydrothermal activities (Murton et al., 2019).

Similarities in lithologies between TAG transection and our SWIR sample set indicate that the findings in SWIR apply to other MORB-hosted high-temperature hydrothermal vents. Our model is also consistent with the finding from terrestrial hydrothermal fields (e.g., Oliva-Urcia et al., 2011). However, it should be noted that the scarce sulfides in our samples hinder further understanding of the coupled hydrothermal alteration and sulfide mineralization. Therefore, comparative rock magnetic investigations on samples with stratigraphic control from other hydrothermal fields are expected to testify and improve this model.

WANG ET AL. 13 of 17



#### 4.3. Implications for Understanding Long-Term Seafloor Magnetization Variations

The long-term magnetization variation of basaltic ocean crust (Bleil & Petersen, 1983) was conventionally explained by a growing CRM at the cost of primary TRM (Masterton et al., 2013; Raymond & LaBrecque, 1987). Low-temperature oxidation of titanomagnetite in oceanic basalts was thought to be responsible for the CRM acquisition (Matzka et al., 2003), but a temporal variation of the oxidation degree is not evident (D. Wang et al., 2005). Seafloor hydrothermal alteration can be an additional mechanism for the replacement of primary TRM with CRM in MORB (Figure 2; Table 2). Our model (Figure 8) bridges the gap between hydrothermal alteration and seafloor magnetization variations. During hydrothermal alteration, equilibrium may not be reached and thus intermediate products such as partially chloritized basalts can exist in ocean crust. Altered MORBs retain magnetization about one order of magnitude lower than fresh MORBs (S. Wang et al., 2020) due to titanomagnetite residues and exsolved magnetite (this study), which is consistent with the one order-of-magnitude magnetization drop for the 0–20 Ma oceanic basalts (Bleil & Petersen, 1983). Detailed rock magnetic and microscopic analyses of various ODP/IODP samples have confirmed the existence of hydrothermal CRM in altered MORBs (e.g., Dekkers et al., 2014; Shau et al., 2000). We therefore speculate that high-temperature hydrothermal alteration can be an underestimated factor that contributes significantly to the profound magnetization drop near mid-ocean ridges.

Although the hydrothermal alteration represents a promising explanation for the long-term seafloor magnetization variations, the intensity of hydrothermal flows is hard to quantify and whether it presents a similar long-term variation pattern remains unknown. Besides, the incidence of hydrothermal fields along mid-ocean ridges is still controversial. Individual vent field, by definition, has a diameter of 10s-1,000s m (Jamieson & Gartman, 2020), while the spacing between vent fields along mid-ocean ridges is much larger. According to the InterRidge Vents Database version 3.4, 404 of 721 seafloor hydrothermal vents discovered to date are located along the >65,000 km mid-ocean ridges (Beaulieu & Szafranski, 2020). Vent occurrence varies along mid-ocean ridges with different spreading rates: slow- and ultraslow-spreading ridges have much larger spacings than fastand intermediate-spreading ridges due to restricted magma supply (Beaulieu et al., 2015). However, it has been challenged by the discoveries that cooling peridotites and serpentinization of mantle rocks can also provide heat to sustain hydrothermal circulations (Baker, 2017). Also, current plume-related surveying methods are insufficient in detecting particle-poor vent fields, and hence the vent population can be significantly underestimated, especially along slow- and ultraslow-spreading mid-ocean ridges (Baker, 2017). Improved strategies, such as applying oxidation-reduction potential sensors in seafloor mapping (e.g., Baker et al., 2016; Chen et al., 2021), have been proved successful in searching for those unheeded hydrothermal flows and for sure will discover more vent fields in future explorations.

In addition to the high-temperature hydrothermal alteration along mid-ocean ridges, low-temperature diffuse flows (<200–250°C; Alt, 1995) in the aged oceanic crust are also essential for the long-term seafloor magnetization variations as they can facilitate the low-temperature oxidation of titanomagnetite (Doubrovine & Tarduno, 2006; O'Reilly, 1984). However, their spatial distribution remains even more poorly understood than the hydrothermal fields along mid-ocean ridges (Baker, 2017). Consequently, although hydrothermal alteration can be a promising mechanism to explain the low-term seafloor magnetization variations, more careful work is needed for verification. In future studies, designing sampling and multidisciplinary investigations may be an important step forward to better understand the effect of hydrothermal alteration on seafloor magnetism.

# 5. Conclusions

We have performed comprehensive rock magnetic and electron microscopic analyses on fresh MORBs, (partially and fully) chloritized basalts, and chloritized basaltic breccias dredged near the SWIR Longqi and Yuhuang hydrothermal fields. Fresh MORBs have large variations in magnetic properties resulting from relative proportions of nano- and micron-scale titanomagnetites. During high-temperature hydrothermal alteration, although primary titanomagnetite was progressively dissolved, secondary magnetite formed in partially chloritized basalts retaining a CRM. A dual Verwey transition signature and coexisting Fe-rich and Ti-rich minerals in partially chloritized basalts indicate that magnetite formed through exsolution and recrystallization during hydrothermal alteration. We established a model to explain the aforementioned magnetomineralogy and magnetic property variations during progressive hydrothermal alteration (Figure 8). Based on this model, hydrothermal alteration is suggested

WANG ET AL. 14 of 17



to potentially contribute to the long-term magnetization variations of oceanic basalts. Our results improve understanding of the rock magnetic mechanism of seafloor hydrothermal alteration, which is important in applying magnetic surveys for prospecting seafloor resources and understanding oceanic geodynamics.

# **Data Availability Statement**

Data sets are available at both the Magnetic Information Consortium (https://www2.earthref.org/MagIC/17130) and the Peking University Open Research Data Platform (https://doi.org/10.18170/DVN/E0ELD5).

#### Acknowledgments

We thank Pengfei Xue and Hoabin Hong for assistance in magnetic measurements and Thomas Berndt for helpful discussions. Constructive reviews by Marco Maffione and one anonymous reviewer have improved this manuscript. We also thank editor Mark Dekkers and associate editor Bjarne Almqvist for editorial handling. This study was supported by the National Key R & D Program of China under contract No. 2018YFC0309901, the National Natural Science Foundation of China (grants 42061130214, 41722402), and COMRA Major Project under contract No. DY135-S1-01-06. Liao Chang acknowledges additional support from a Royal Society-Newton Advanced Fellowship (NAF\R1\201096). Shishun Wang acknowledges a Visiting Research Fellowship from the Institute for Rock Magnetism (IRM), University of Minnesota. The IRM is a US National Multi-user Facility supported through the Instrumentation and Facilities Program of the National Science Foundation, Earth Sciences Division, and by funding from the University of Minnesota. This is IRM publication #2105.

#### References

- Ade-Hall, J. M., Palmer, H. C., & Hubbard, T. P. (1971). The magnetic and opaque petrological response of basalts to regional hydrothermal alteration. *Geophysical Journal of the Royal Astronomical Society*, 24(2), 137–174. https://doi.org/10.1111/j.1365-246X.1971.tb02171.x
- Almeida, T. P., Kasama, T., Muxworthy, A. R., Williams, W., Nagy, L., Hansen, T. W., et al. (2014). Visualized effect of oxidation on magnetic recording fidelity in pseudo-single-domain magnetite particles. *Nature Communications*, 5, 5154. https://doi.org/10.1038/ncomms6154
- Alt, J. C. (1995). Subseafloor processes in mid-ocean ridge hydrothermal systems. Seafloor hydrothermal systems: Physical, chemical, biological, and geological interactions, Geophysical Monograph series (Vol. 91, pp. 85–114). American Geophysical Union. https://doi.org/10.1029/
- Bai, F., Chang, L., Berndt, T. A., & Pei, Z. (2021). Micromagnetic calculations of the effect of magnetostatic interactions on isothermal remanent magnetization curves: Implications for magnetic mineral identification. *Journal of Geophysical Research: Solid Earth*, 126, e2021JB022335. https://doi.org/10.1029/2021JB022335
- Baker, E. T. (2017). Exploring the ocean for hydrothermal venting: New techniques, new discoveries, new insights. *Ore Geology Reviews*, 86, 55–69. https://doi.org/10.1016/j.oregeorev.2017.02.006
- Baker, E. T., Resing, J. A., Haymon, R. M., Tunnicliffe, V., Lavelle, J. W., Martinez, F., et al. (2016). How many vent fields? New estimates of vent field populations on ocean ridge from precise mapping of hydrothermal discharge locations. *Earth and Planetary Science Letters*, 449, 186–196. https://doi.org/10.1016/j.epsl.2016.05.031
- Beaulieu, S. E., Baker, E. T., & German, C. R. (2015). Where are the undiscovered hydrothermal vents on oceanic spreading ridges? *Deep-Sea Research II*, 121, 202–212. https://doi.org/10.1016/j.dsr2.2015.05.001
- Beaulieu, S. E., & Szafranski, K. (2020). Interridge global database of active submarine hydrothermal vent fields. Retrieved from http://vents-data.interridge.org
- Berndt, T. A., & Chang, L. (2019). Waiting for Forcot: Accelerating FORC processing 100x using a fast-Fourier-transform algorithm. *Geochemistry, Geophysics, Geosystems*, 20, 6223–6233. https://doi.org/10.1029/2019GC008380
- Bilardello, D. (2020). Practical magnetism II: Humps and a bump, the maghemite song. IRM Quarterly, 30(1), 1-16.
- Bleil, U., & Petersen, N. (1983). Variations in magnetization intensity and low-temperature titanomagnetite oxidation of ocean floor basalts. Nature, 301, 384–388, https://doi.org/10.1038/301384a0
- Bowles, J. A., Jackson, M., Chen, A., & Solheid, P. (2009). Interpretation of low-temperature data part I: Superparamagnetism and paramagnetism. *The IRM Quarterly*, 19(3), 1–11.
- Bowles, J. A., Morris, A., Tivey, M. A., & Lascu, I. (2020). Magnetic mineral populations in lower oceanic crustal gabbros (Atlantis bank, SW Indian ridge): Implications for marine magnetic anomalies. Geochemistry, Geophysics, Geosystems, 21, e2019GC008847. https://doi.org/10.1029/2019GC008847
- Chang, L., Harrison, R. J., & Berndt, T. A. (2019). Micromagnetic simulation of magnetofossils with realistic size and shape distributions: Linking magnetic proxies with nanoscale observations and implications for magnetofossil identification. Earth and Planetary Science Letters, 527, 115790. https://doi.org/10.1016/j.epsl.2019.115790
- Chang, L., Hong, H., Bai, F., Wang, S., Pei, Z., Paterson, G. A., et al. (2021). Detrital remanent magnetization of single-crystal silicates with magnetic inclusions: Constraints from deposition experiments. *Geophysical Journal International*, 224(3), 2001–2015. https://doi.org/10.1093/gji/ggaa559
- Chen, S., Tao, C., & German, C. R. (2021). Abundance of low-temperature axial venting at the equatorial East Pacific Rise. *Deep-Sea Research* 1, 167, 103426. https://doi.org/10.1016/j.dsr.2020.103426
- Chesworth, W., Dejou, J., & Larroque, P. (1981). The weathering of basalt and relative mobilities of the major elements at Belbex, France. Geochimica et Cosmochimica Acta, 45(7), 1235–1243. https://doi.org/10.1016/0016-7037(81)90147-2
- Church, N., Feinburg, J. M., & Harrison, R. (2011). Low-temperature domain wall pinning in titanomagnetite: Quantitative modeling of multi-domain first-order reversal curve diagrams and AC susceptibility. Geochemistry, Geophysics, Geosystems, 12(7), Q07Z27. https://doi.org/10.1029/2011GC003538
- Dekkers, M. J., Heslop, D., Herrero-Bervera, E., Acton, G., & Krása, D. (2014). Insights into magmatic processes and hydrothermal alteration of in situ superfast spreading ocean crust at ODP/IODP site 1256 from a cluster analysis of rock magnetic properties. *Geochemistry, Geophysics, Geosystems*, 15(8), 3430–3447. https://doi.org/10.1002/2014GC005343
- Dick, H. J. B., Lin, J., & Schouten, H. (2003). An ultraslow-spreading class of ocean ridge. Nature, 426, 405–412. https://doi.org/10.1038/nature02128
- Doubrovine, P. V., & Tarduno, J. A. (2004). Self-reversed magnetization carried by titanomagnemite in oceanic basalts. *Earth and Planetary Science Letters*, 222(3–4), 959–969. https://doi.org/10.1016/j.epsl.2004.04.009
- Doubrovine, P. V., & Tarduno, J. A. (2006). Alteration and self-reversal in oceanic basalts. *Journal of Geophysical Research*, 111, B12S30. https://doi.org/10.1029/2006JB004468
- Egli, R. (2003). Analysis of the field dependence of remanent magnetization curves. *Journal of Geophysical Research*, 108(B2), 2081. https://doi.org/10.1029/2002JB002023
- Fabian, K. (2006). Approach to saturation analysis of hysteresis measurements in rock magnetism and evidence for stress dominated magnetic anisotropy in young mid-ocean ridge basalt. *Physics of the Earth and Planetary Interiors*, 154, 299–307. https://doi.org/10.1016/j.pepi.2005.06.016

WANG ET AL. 15 of 17



- Galley, C. G., Jamieson, J. W., Lelièvre, P. G., Farquharson, C. G., & Parianos, J. M. (2020). Magnetic imaging of subseafloor hydrothermal fluid circulation pathways. *Science Advances*, 6(44), eabc6844. https://doi.org/10.1126/sciadv.abc6844
- Gee, J. S., & Kent, D. V. (2007). Source of oceanic magnetic anomalies and the geomagnetic polarity timescale. *Treatise on Geophysics*, 5, 419–460. https://doi.org/10.1016/B978-0-444-53802-4.00106-8
- Harrison, R. J., & Putnis, A. (1999). Determination of the mechanism of cation ordering in magnesioferrite (MgFe<sub>2</sub>O<sub>4</sub>) from the time- and temperature-dependence of magnetic susceptibility. *Physics and Chemistry of Minerals*, 26, 322–332. https://doi.org/10.1007/s002690050192
- Honnorez, J. J., Alt, J. C., & Humphris, S. E. (1998). Vivisection and autopsy of active and fossil hydrothermal alterations of basalt beneath and within the TAG hydrothermal mound. In P. M. Herzig, S. E. Humphris, D. J. Miller, & R. A. Zierenberg (Eds.), *Proceedings of the ocean drilling program, Scientific results* (Vol. 158, pp. 231–254). https://doi.org/10.2973/odp.proc.sr.158.219.1998
- Humphris, S. E., Herzig, P. M., Miller, D. J., Alt, J. C., Becker, K., Brown, D., et al. (1995). The internal structure of an active sea-floor massive sulphide deposit. *Nature*, 377, 713–716. https://doi.org/10.1038/377713a0
- Humphris, S. E., Herzig, P. M., Miller, D. J., & Shipboard Scientific Party. (1996). Proceedings of the ocean drilling program. Initial Reports, 158. Ocean Drilling Program. https://doi.org/10.2973/odp.proc.ir.158.1996
- Iwasaki, T., Mizutani, N., Watano, S., Yanagida, T., & Kawai, T. (2012). Hydrothermal synthesis of magnetite nanoparticles via sequential formation of iron hydroxide precipitates. *Journal of Experimental Nanoscience*, 7(4), 355–365. https://doi.org/10.1080/17458080.2010.515250
- Jamieson, J. W., & Gartman, A. (2020). Defining active, inactive, and extinct seafloor massive sulfide deposits. Marine Policy, 117, 103926. https://doi.org/10.1016/j.marpol.2020.103926
- Just, J., & Kontny, A. (2012). Thermally induced alterations of minerals during measurements of the temperature dependence of magnetic susceptibility: A case study from the hydrothermally altered Soultz-sous-Forêts granite, France. *International Journal of Earth Sciences*, 101, 819–839. https://doi.org/10.1007/s00531-011-0668-9
- Kakol, Z., Sabol, J., & Honig, J. M. (1991). Magnetic anisotropy of titanomagnetites Fe<sub>3-x</sub>Ti<sub>x</sub>O<sub>4</sub>, 0≤x≤0.55. Physical Review B, 44, 2198. https://doi.org/10.1103/PhysRevB.44.2198
- Kontny, A., & Grothaus, L. (2017). Effects of shock pressure and temperature on titanomagnetite from ICDP cores and target rocks of the El'gygytgyn impact structure, Russia. *Studia Geophysica et Geodaetica*, 61, 162–183. https://doi.org/10.1007/s11200-016-0819-3
- Krása, D., & Herrero-Bervera, E. (2005). Alteration induced changes of magnetic fabric as exemplified by dykes of the Koolau volcanic range. Earth and Planetary Science Letters, 240, 445–453. https://doi.org/10.1016/j.epsl.2005.09.028
- Krása, D., & Matzka, J. (2007). Inversion of titanomaghemite in oceanic basalt during heating. Physics of the Earth and Planetary Interiors, 160, 169–179. https://doi.org/10.1016/j.pepi.2006.11.004
- Lascu, I., Einsle, J. F., Ball, M. R., & Harrison, R. J. (2018). The vortex state in geologic materials: A micromagnetic perspective. *Journal of Geophysical Research: Solid Earth*, 123, 7285–7304. https://doi.org/10.1029/2018JB015909
- Liao, S., Tao, C., Li, H., Barriga, F. J. A. S., Liang, J., Yang, W., et al. (2018). Bulk geochemistry, sulfur isotope characteristics of the Yuhuang-1 hydrothermal field on the ultraslow-spreading Southwest Indian Ridge. Ore Geology Reviews, 96, 13–27. https://doi.org/10.1016/j.oregeorev.2018.04.007
- Liu, Q., Yu, Y., Torrent, J., Roberts, A. P., Pan, Y., & Zhu, R. (2006). Characteristic low-temperature magnetic properties of aluminous goethite [α-(Fe, Al)OOH] explained. *Journal of Geophysical Research*, 111, B12S34. https://doi.org/10.1029/2006JB004560
- Lurcock, P. C., & Wilson, G. S. (2012). PuffinPlot: A versatile, user-friendly program for paleomagnetic analysis. Geochemistry, Geophysics, Geosystems, 13, Q06Z45. https://doi.org/10.1029/2012GC004098
- Masterton, S. M., Gubbins, D., Müller, R. D., & Singh, K. H. (2013). Forward modelling of oceanic lithospheric magnetization. *Geophysical Journal International*, 192(3), 951–962. https://doi.org/10.1093/gji/ggs063
- Matzka, J., Krása, D., Kunzmann, T., Schult, A., & Petersen, N. (2003). Magnetic state of 10–40 Ma old ocean basalts and its implications for natural remanent magnetization. Earth and Planetary Science Letters, 206(3–4), 541–553. https://doi.org/10.1016/S0012-821X(02)01094-4
- Maxbauer, D. P., Feinberg, J. M., & Fox, D. L. (2016). MAX Unmix: A web application for unmixing magnetic coercivity distributions. Computers & Geosciences, 95, 140–145. https://doi.org/10.1016/j.cageo.2016.07.009
- Morin, F. J. (1950). Magnetic susceptibility of  $\alpha Fe_2O_3$  and  $\alpha Fe_2O_3$  with added titanium. *Physical Review*, 78, 819–820. https://doi.org/10.1103/PhysRev.78.819.2
- Moskowitz, B. M., Jackson, M., & Kissel, C. (1998). Low-temperature magnetic behavior of titanomagnetites. Earth and Planetary Science Letters, 157, 141–149. https://doi.org/10.1016/S0012-821X(98)00033-8
- Murton, B. J., Lehrmann, B., Dutrieux, A. M., Martins, S., de la Iglesia, A. G., Stobbs, I. J., et al. (2019). Geological fate of seafloor massive sulphides at the TAG hydrothermal field (Mid-Atlantic Ridge). Ore Geology Reviews, 107, 903–925. https://doi.org/10.1016/j.oregeorev.2019.03.005
- Nagata, T. (1961). Rock magnetism. Maruzen Company.
- Newell, A. J. (2005). A high-precision model of first-order reversal curve (FORC) functions for single-domain ferromagnets with uniaxial anisotropy. Geochemistry, Geophysics, Geosystems, 6, Q05010. https://doi.org/10.1029/2004GC000877
- Nikolaisen, E. S., Harrison, R. J., Fabian, K., & McEnroe, S. A. (2020). Hysteresis of natural magnetite ensembles: Micromagnetics of silicate-hosted magnetite inclusions based on focused-ion-beam nanotomography. *Geochemistry, Geophysics, Geosystems*, 21, e2020GC009389. https://doi.org/10.1029/2020GC009389
- Oliva-Urcia, B., Kontny, A., Vahle, C., & Schleicher, A. M. (2011). Modification of the magnetic mineralogy in basalts due to interactions in a high-temperature geothermal system (Krafla, Iceland). *Geophysical Journal International*, 186(1), 155–174. https://doi.org/10.1111/j.1365-246X.2011.05029.x
- O'Reilly, W. (1984). Rock and mineral magnetism. Blackie & Son. Ltd.
- Özdemir, Ö., & Dunlop, D. J. (1985). An experiment study of chemical remanent magnetizations of synthetic monodomain titanomaghemites with initial thermoremanent magnetizations. *Journal of Geophysical Research*, 90(B13), 11513–11523. https://doi.org/10.1029/JB090iB13p11513 Özdemir, Ö., Dunlop, D. J., & Berquó, T. S. (2008). Morin transition in hematite: Size dependence and thermal hysteresis. *Geochemistry, Geo-*
- physics, Geosystems, 9, Q10Z01. https://doi.org/10.1029/2008GC002110
- Pan, Y., Liu, Q., Deng, C., Qin, H., & Zhu, R. (2006). Thermally induced inversion of Al-substituted titanomagnetite in basalt: Evidence for partial self-reversal. *Journal of Geophysical Research*, 111, B12S29. https://doi.org/10.1029/2006JB004576
- Paterson, G. A., Zhao, X., Jackson, M., & Heslop, D. (2018). Measuring, processing, and analyzing hysteresis data. Geochemistry, Geophysics, Geosystems, 19, 1925–1945. https://doi.org/10.1029/2018GC007620
- Petersen, N., Eisenach, P., & Bleil, U. (1979). Low temperature alteration of the magnetic minerals in ocean floor basalts. In M. Talwani, C. G. Harrison, & D. E. Hayes (Eds.), *Deep drilling results in the Atlantic Ocean: Ocean crust. Maurice Ewing series* (Vol. 2, pp. 169–209), American Geophysical Union. https://doi.org/10.1029/ME002p0169

WANG ET AL. 16 of 17



- Pochon, A., Beaudoin, G., Branquet, Y., Boulvais, P., Gloaguen, E., & Gapais, D. (2017). Metal mobility during hydrothermal breakdown of Fe-Ti oxides: Insights from Sb-Au mineralizing event (Variscan Armorican Massif, France). Ore Geology Reviews, 91, 66–99. https://doi. org/10.1016/j.oregeorev.2017.10.021
- Pontesilli, A., Masotta, M., Nazzari, M., Mollo, S., Armienti, P., Scarlato, P., & Brenna, M. (2019). Crystallization kinetics of clinopyroxene and titanomagnetite growing from a trachybasaltic melt: New insights from isothermal time-series experiments. *Chemical Geology*, 510, 113–129. https://doi.org/10.1016/j.chemgeo.2019.02.015
- Raymond, C. A., & LaBrecque, J. L. (1987). Magnetization of the oceanic crust: Thermoremanent magnetization or chemical remanent magnetization? *Journal of Geophysical Research*, 92(B8), 8077–8088. https://doi.org/10.1029/JB092iB08p08077
- Roberts, A. P., Almeida, T. P., Church, N. S., Harrison, R. J., Heslop, D., Li, Y., et al. (2017). Resolving the origin of pseudo-single domain magnetic behavior. *Journal of Geophysical Research: Solid Earth*, 122, 9534–9558. https://doi.org/10.1002/2017JB014860
- Roberts, A. P., Heslop, D., Zhao, X., & Pike, C. R. (2014). Understanding fine magnetic particle systems through use of first-order reversal curve diagrams. Reviews of Geophysics, 52, 557–602. https://doi.org/10.1002/2014RG000462
- Roberts, A. P., Pike, C. R., & Verosub, K. L. (2000). First-order reversal curve diagrams: A new tool for characterizing the magnetic properties of natural samples. *Journal of Geophysical Research*, 105(B12), 28461475–28461528. https://doi.org/10.1029/2000JB900326
- Roberts, A. P., Tauxe, L., Heslop, D., Zhao, X., & Jiang, Z. (2018). A critical appraisal of the "Day" diagram. *Journal of Geophysical Research:* Solid Earth, 123, 2618–2644. https://doi.org/10.1002/2017JB015247
- Ruiz-Agudo, E., Putnis, C. V., & Putnis, A. (2014). Coupled dissolution and precipitation at mineral-fluid interfaces. Chemical Geology, 383, 132–146. https://doi.org/10.1016/j.chemgeo.2014.06.007
- Shaar, R., & Feinberg, J. M. (2013). Rock magnetic properties of dendrite: Insights from MFM imaging and implications for paleomagnetic studies. Geochemistry, Geophysics, Geosystems, 14, 407–421. https://doi.org/10.1002/ggge.20053
- Shau, Y.-H., Torii, M., Horng, C.-S., & Peacor, D. R. (2000). Subsolidus evolution and alteration of titanomagnetite in ocean Ridge Basalts from deep sea drilling Project/Ocean Drilling Program Hole 504B, Leg 83: Implications for the timing of magnetization. *Journal of Geophysical Research*, 105(B1023), 635649–635723. https://doi.org/10.1029/2000JB900191
- Stefánsson, A. (2001). Dissolution of primary minerals of basalt in natural waters I. calculations of mineral solubilities from 0°C to 350°C. Chemical Geology, 172, 225–250. https://doi.org/10.1016/S0009-2541(00)00263-1
- Stefánsson, A., Gíslason, S. R., & Arnórsson, S. (2001). Dissolution of primary minerals in natural waters II. Mineral saturation state. Chemical Geology, 172, 251–276. https://doi.org/10.1016/S0009-2541(00)00262-X
- Szitkar, F., Dyment, J., Choi, Y., & Fouquet, Y. (2014). What causes low magnetization at basalt-hosted hydrothermal sites? Insights from inactive site Krasnov (MAR 16°38' N). Geochemistry, Geophysics, Geosystems, 15(4), 1441–1451. https://doi.org/10.1002/2014GC005284
- Tao, C., Lin, J., Guo, S., Chen, Y. J., Wu, G., Han, X., et al. (2012). First active hydrothermal vents on an ultraslow-spreading center: Southwest Indian Ridge. *Geology*, 40(1), 47–50. https://doi.org/10.1130/G32389.1
- Tao, C., Seyfried, W. E., Lowell, R. P., Liu, Y., Liang, J., Guo, Z., et al. (2020). Deep high-temperature hydrothermal circulation in a detachment faulting system on the ultra-slow spreading ridge. *Nature Communications*, 11, 1300. https://doi.org/10.1038/s41467-020-15062-w
- Tauxe, L., Bertram, H. N., & Seberino, C. (2002). Physical interpretation of hysteresis loop: Micromagnetic modeling of fine particle magnetite. Geochemistry, Geophysics, Geosystems, 3(10), 1055. https://doi.org/10.1029/2001GC000241
- Till, J. L., Jackson, M. J., Rosenbaum, J. G., & Solheid, P. (2011). Magnetic properties in an ash flow tuff with continuous grain size variation: A natural reference for magnetic particle granulometry. Geochemistry, Geophysics, Geosystems, 12(7), Q07Z26. https://doi.org/10.1029/2011GC003648
- Tivey, M. A., & Johnson, H. P. (2002). Crustal magnetization reveals subsurface structure of Juan de Fuca Ridge hydrothermal vent fields. *Geology*, 30(11), 9792–9982. https://doi.org/10.1130/0091-7613(2002)030<0979:CMRSSO>2.0
- Tivey, M. K. (2007). Generation of seafloor hydrothermal vent fluids and associated mineral deposits. *Oceanography*, 20(1), 50–65. https://doi.org/10.5670/oceanog.2007.80
- Verwey, E. J. W. (1939). Electronic conduction of magnetite (Fe<sub>3</sub>O<sub>4</sub>) and its transition point at low temperatures. *Nature*, 144, 327–328. https://doi.org/10.1038/144377b0
- Wang, D., & Van der Voo, R. (2004). The hysteresis properties of multidomain magnetite and titanomagnetite/titanomagnemite in mid-ocean ridge basalts. Earth and Planetary Science Letters, 220, 175–184. https://doi.org/10.1016/S0012-821X(04)00052-4
- Wang, D., Van der Voo, R., & Peacor, D. R. (2005). Why is the remanent magnetic intensity of Cretaceous MORB so much higher than that of mid to late Cenozoic MORB? *Geosphere*, 1(3), 138–146. https://doi.org/10.1130/GES00024.1
- Wang, S., Chang, L., Wu, T., & Tao, C. (2020). Progressive dissolution of titanomagnetite in high-temperature hydrothermal vents dramatically reduces magnetization of basaltic ocean crust. *Geophysical Research Letters*, 47(8), e2020GL087578. https://doi.org/10.1029/2020GL087578
- Xu, W., Peacor, D. R., Dollase, W. A., Van der Voo, R., & Beaubouef, R. (1997). Transformation of titanomagnetite to titanomagnetite: A slow, two-step, oxidation-ordering process in MORB. American Mineralogist, 82, 1101–1110. https://doi.org/10.2138/am-1997-11-1207
- Zhou, W., Van der Voo, R., Peacor, D. R., Wang, D., & Zhang, Y. (2001). Low-temperature oxidation in MORB of titanomagnetite to titanomagnetie: A gradual process with implications for marine magnetic anomaly amplitudes. *Journal of Geophysical Research*, 106(B4), 6409–6421. https://doi.org/10.1029/2000JB900447
- Zhou, W., Van der Voo, R., Peacor, D. R., & Zhang, Y. (2000). Variable Ti-content and grain size of titanomagnetite as a function of cooling rate in very young MORB. Earth and Planetary Science Letters, 179, 9–20. https://doi.org/10.1016/S0012-821X(00)00100-X

WANG ET AL. 17 of 17